ELSEVIER

Physica D 137 (2000) 277–294

PHYSICA D

www.elsevier.com/locate/physd

Dissipative behavior of some fully non-linear KdV-type equations

Yann Brenier [a], Doron Levy [b,*]

[a] *Université Pierre et Marie Curie, 4 Place Jussieu, 75252 Paris Cedex 05, France*

[b] *Department of Mathematics, University of California, and Lawrence Berkeley National Lab, Berkeley, CA 94720, USA*

Received 5 May 1999; received in revised form 26 July 1999; accepted 30 August 1999

Communicated by I. Gabitov

Abstract

The KdV equation can be considered as a special case of the general equation $u_t + f(u)_x - \delta g(u_{xx})_x = 0,\ \delta > 0$, where f is non-linear and g is linear, namely $f(u) = u^2/2$ and $g(v) = v$. As the parameter δ tends to 0, the dispersive behavior of the KdV equation has been throughly investigated (see, e.g., [P.G. Drazin, Solitons, London Math. Soc. Lect. Note Ser. 85, Cambridge University Press, Cambridge, 1983; P.D. Lax, C.D. Levermore, The small dispersion limit of the Korteweg–de Vries equation, III, Commun. Pure Appl. Math. 36 (1983) 809–829; G.B. Whitham, Linear and Nonlinear Waves, Wiley/Interscience, New York, 1974] and the references therein). We show through numerical evidence that a completely different, dissipative behavior occurs when g is non-linear, namely when g is an even concave function such as $g(v) = -|v|$ or $g(v) = -v^2$. In particular, our numerical results hint that as $\delta \to 0$ the solutions *strongly converge* to the unique entropy solution of the formal limit equation, in total contrast with the solutions of the KdV equation.

PACS: 05.45.−a; 02.70.Bf

Keywords: KdV-type equations; Finite-difference methods; Nonlinear dynamics

1. Introduction

Let us consider the first-order non-linear evolution PDE

$$u_t + f(u)_x = 0, \tag{1.1}$$

with a strictly convex non-linearity $f''(u) \geq \alpha > 0$, typically $f(u) = u^2/2$ which corresponds to the usual inviscid Burgers equation [11]. This equation generally produces shock waves in a finite time and solutions must be understood in a suitable weak sense. A good framework enforcing existence, uniqueness, L^1 stability, (see, e.g.,

* Corresponding author.

E-mail addresses: brenier@dmi.ens.fr (Y. Brenier), dlevy@math.berkeley.edu (D. Levy).

0167-2789/00/$ – see front matter
PII: S0167-2789(99)00190-6

[8–10]) is provided by the so-called entropy solutions, obtained through the vanishing viscosity method by passing to the limit in the viscous approximation

$$u_t + f(u)_x - \delta u_{xx} = 0, \tag{1.2}$$

as $\delta > 0$ tends to zero [10]. Entropy solutions can be also characterized as the weak solutions of (1.1) which satisfy the Oleinik one-sided Lipschitz condition (OSLC)

$$u_x(t, x) \leq \frac{1}{\alpha t}. \tag{1.3}$$

A behavior completely different from (1.3) is observed if (1.1) is approximated by the KdV equation

$$u_t + f(u)_x - \delta u_{xxx} = 0, \quad \delta > 0, \tag{1.4}$$

as investigated by many authors, in particular Lax and Levermore [6]. When the formal limit has shocks, the corresponding solution of the KdV equation becomes highly oscillatory and does not converge at all to the entropy solution (even in a weak sense).

An alternative approach of approximating equations such as (1.1) is to design a numerical scheme. In [1] Brenier and Osher presented a second-order accurate version of the Roe scheme [8,10] and an OSLC consistent method of lines for approximating solutions of scalar conservation laws, (1.1). As was already pointed out in [1], the "modified equation" of this scheme (that is to say the asymptotic PDE of the discrete equation) is of interest since (as it is second-order) it must involve, just like the KdV equation, a third-order term, but unlike the KdV equation, due to the enforced OSLC this third-order term must enforce restrictions on the possible creation of wiggles. Our present work presents an extended numerical study of these "non-classical dispersive" effects, as well as an extended study of the numerics involved.

The model equations we consider are

$$u_t + f(u)_x - \delta g(u_{xx})_x = 0, \quad \delta > 0, \tag{*}$$

where g is concave and even, typically $g(s) = -|s|$ or the smoother $g(s) = -s^2$. The KdV equation can be considered as a special case of (*) where f is non-linear and g is linear, namely $f(u) = u^2/2$ and $g(u) = v$. The numerical tools taken from [1] enable us to approximate the solutions of (*) with a numerical method in which its modified equation takes the desired form of

$$u_t + f(u)_x - \delta g(u_{xx})_x = -\epsilon u_{xxxx} + \text{LOT}, \tag{1.5}$$

with a positive $\epsilon \sim \delta \Delta x$, where LOT means perturbation terms with at most third-order space derivatives (low order terms). In the specific case where $g(s) = -|s|$, there are no low order terms on the RHS of (1.5) and hence we are left only with a *linear* dissipative term proportional to $\delta \Delta x$, which enables us to hold a fixed δ while eliminating the RHS at the limit $\epsilon \to 0$.

The analytical tools available to study fully non-liner evolution PDEs such as (*) and (1.5), seem to be limited and a rigorous theory is, in our opinion, a very challenging task that deserves to be further addressed. Our main results are based on numerical evidence.

The simple *non-linear switch* in the third-order term $|u_{xx}|_x$ based on the sign of the second derivative u_{xx}, has a major impact. The same holds true for other non-linear third-order operators such as $(u_{xx}^2)_x$. Instead of the usual dispersive wave-train that develops in the KdV equation, here we still observe the appearance of a *single* ripple, which indeed can be still considered as a dispersive phenomenon. This ripple, however, is of a totally different character than what we are familiar with in the KdV equation. Instead of developing into a full wave-train which

propagates in time, this ripple remains *single* during the evolution of the solution. It does not increase above a certain size which is related to the value of the parameter δ in (*).

The striking numerical discovery is that not only this ripple is single, but it also *disappears* in the limit $\delta \to 0$. It turns that (*) is much closer in its behavior to the dissipative, viscous approximations of the form

$$u_t + f(u)_x = \epsilon u_{xx}, \quad \epsilon > 0,$$

than to the KdV equation

$$u_t + f(u)_x + \delta u_{xxx} = 0,$$

for which at the same limit $\delta \to 0$, the dispersive waves increase.

The natural conjecture that follows is that (1.5), *strongly converges* to the entropy solution of the scalar conservation law (1.1) as δ and $\epsilon\delta^{-1}$ tend to 0.

We would like to emphasize that when using numerical methods in order to approximate solutions of differential equations, instead of solving the original problem, we end up solving a modified problem, which typically includes high-order terms. Here, we are interested in studying the effects of such high-order terms in the particular case in hand. We believe that the properties of the model equations we study in this work, might provide insight for the inclusion of similar nonlinear terms in future models.

The paper is organized as follows: we start in Section 2 by presenting both our model equations and the numerical method of approximating their solutions. We continue in Section 3 by commenting on the major properties of these equations. In particular, we study traveling waves solutions and state a formal one-sided bound (OSLC-type) on the derivative.

We then continue in Section 4 by presenting several numerical examples which leads us to our main conjecture stated above, which is formalized in Conjecture 4.1.

We end in Section 5 by demonstrating and analyzing spurious numerical oscillations that appear when solving our model problems with a certain choice of parameters. The methods we use for analyzing the binary oscillations follow Goodman and Lax [3]. Similar techniques were used, e.g., in [4,5,7]. This study is aimed at gaining a further understanding in order to be able to distinguish between the properties of the equations and the appearing numerical phenomena which depend on the specific method used when approximating the solutions.

2. Motivation

2.1. The model equations

The motivation for our study is the modified equation of the Brenier-Osher (BO) scheme presented in [1]. We start by considering the scalar conservation law (1.1) with a (strictly) convex flux function, $f''(u) \geq \alpha > 0$.

We discretize the space using a fixed mesh spacing, Δx, denoting the approximation of the solution at the discrete grid-points by $u_i := u(i\Delta x)$.

The BO method for approximating solutions of (1.1) is a second-order convergent Roe scheme and an OSLC consistent method of lines, which can be written as

$$\frac{\mathrm{d}u_i}{\mathrm{d}t} + \frac{1}{\Delta x}(f_{i+1/2} - f_{i-1/2}) = 0, \tag{2.1}$$

with

$$f_{i+1/2} = h\left(u_i + \frac{\Delta x}{2}s_i, u_{i+1} - \frac{\Delta x}{2}s_{i+1}\right).$$

Here, h is the Godunov flux associated with f,

$$h(a,b) = h_{\mathrm{GOD}}(a,b) = \epsilon \min_{0\le s\le 1} \epsilon f(a + s(b-a)), \quad \epsilon = \mathrm{sgn}(b-a),$$

and the slopes, s_i, are limited by

$$s_i = \frac{1}{\Delta x}\max(u_{i+1} - u_i, u_i - u_{i-1}).$$

We note that the OSLC consistency of (2.1) is in the sense that the discrete approximation satisfies

$$\frac{u_{i+1}(t) - u_i(t)}{\Delta x} \le \frac{1}{p(u(0,\cdot))^{-1} + \alpha t},$$

where $p(v)$ is the one-sided Lipschitz semi-norm,

$$p(v) = \sup_{x\neq y}\left(\frac{v(x) - v(y)}{x - y}\right)_+, \qquad a_+ = \max(0, a).$$

In the linear case, i.e. for $f(u) = \beta u$ with β constant, the BO scheme yields the modified equation

$$u_t + f(u)_x + \delta |u_{xx}|_x = 0, \qquad \delta = \mathrm{O}(\Delta x^2). \tag{2.2}$$

In the nonlinear case for a general $f(u)$, additional low-order terms appear in (2.2). The existence of these terms was ignored in [1].

As was already pointed out in [1], this modified equation (2.2) is of interest since it involves a dispersion term (as it is second-order), but unlike KdV, due to the enforced OSLC, this third-order term does not create wiggles. These are the properties this work is aimed at studying.

Since (2.2) includes a non-smooth flux, we extend the current discussion to a wider family

$$u_t + f(u)_x - \delta g(u_{xx})_x = 0, \tag{2.3}$$

where $g(u_{xx})$ is assumed to be concave, $g''(s) < 0, \forall s$. There are no further regularity assumptions on g.

To summarize, our model equations are (2.2) and its smooth version (2.3).

2.2. The numerical scheme

For the following analysis the precise derivation and the origin of (2.2) and (2.3) is no longer important. It is their properties that we want to study. To proceed, we write a discretization of (2.2) and (2.3). It is remarkable that it is possible to write down such a discretization whose modified equation involved a *linear* fourth-order derivative of the "correct" (dissipative) sign.

Following [1], a straightforward discretization of the generalized modified equation (2.3) will be, e.g., to define the (first-order) numerical flux $g_{i+1/2} = g(w_i, w_{i+1})$ as the Engquist–Osher (EO) flux

$$g_{\mathrm{EO}}(a,b) = g(b_+) + g(a_-), \qquad b_+ = \max(0,b), \quad a_- = \min(0,a). \tag{2.4}$$

A method of lines for (2.3) can be then written as

$$\Delta x \frac{\mathrm{d}u_i}{\mathrm{d}t} + \Delta_-\left[f\left(\frac{u_i + u_{i+1}}{2}\right) - \delta g(w_i, w_{i+1})\right] = 0, \tag{2.5}$$

where $\Delta_- a_i = a_i - a_{i-1}$, and $w_i = (u_{i-1} - 2u_i + u_{i+1})/(\Delta x)^2$.

Replacing the time derivative in (2.5) by the forward-Euler discretization associated with a fixed time-step, Δt, we obtain the fully-discrete

$$\frac{u_i^{n+1}-u_i^n}{\Delta t}+\frac{1}{\Delta x}\Delta_-\left[f\left(\frac{u_i^n+u_{i+1}^n}{2}\right)-\delta g(w_i^n, w_{i+1}^n)\right]=0, \tag{2.6}$$

where for the space-time discretization we use the notation $u_i^n := u(i\Delta x, n\Delta t)$.

A somewhat tedious but straightforward computation shows that the limiting equation for the fully-discrete process (2.6) has the form

$$u_t+f(u)_x-\delta g(u_{xx})_x=\Delta x\delta[\tfrac{1}{2}\mathrm{sgn}(u_{xx})g'(u_{xx})u_{xxxx}+\tfrac{1}{2}\mathrm{sgn}(u_{xx})g''(u_{xx})u_{xxx}^2]+\mathrm{O}((\Delta x)^2,\Delta t). \tag{2.7}$$

In particular, for the choice $g(s)=-|s|$, (2.7) becomes

$$u_t+f(u)_x+\delta|u_{xx}|_x=-\epsilon u_{xxxx}, \qquad \epsilon=\tfrac{1}{2}\Delta x\delta. \tag{2.8}$$

For the more regular choice of $g(s)=-s^2$, (2.7) takes the form of

$$u_t+f(u)_x+\delta(u_{xx}^2)_x=-\Delta x\delta[|u_{xx}|u_{xxxx}+\tfrac{1}{2}\mathrm{sgn}(u_{xx})u_{xxx}^2]. \tag{2.9}$$

At that point, we add Eqs. (2.8) and (2.9) to our two previous model equations, (2.2) and (2.3).

3. Properties of the model equation

In this section we discuss some of the major properties of (2.3). We will assume that $f(u)$ is convex. For demonstration purposes it will be usually taken as $f(u)=u^2/2$. We also assume a concave $g(s)$, which will be either $-|s|$ or $-s^2$, unless mentioned otherwise. Namely, we deal with two model equations. The first equation corresponds to the choice of $g(s)=-|s|$,

$$u_t+uu_x+\delta|u_{xx}|_x=0. \tag{3.1}$$

The second choice corresponds to the smoother, $g(s)=-s^2$,

$$u_t+uu_x+\delta(u_{xx}^2)_x=0. \tag{3.2}$$

We note that in both equations (3.1) and (3.2), one can eliminate by rescaling the parameter δ. This is done in (3.1) by the rescaling $u\to\delta u$ and $t\to\delta t$. Such a rescaling also holds for (2.8) when $\epsilon\sim\delta\Delta x$. The different scaling $x\to\delta^{-1/4}x$ and $t\to\delta^{-1/4}t$ gets rid of δ in (3.2).

We would also like to note that $u_t+uu_x+\delta g(u_{xx})_x=-\epsilon u_{xxxx}$ is invariant under the Galilean transformation $u(x,t)\to u(x+ct,t)$ and $u\to u-c$.

3.1. Traveling waves

We compute a monotonic profile of the traveling waves solution for (3.2). The monotonicity is an important property of these traveling waves. Our numerical experiments below indicate that these particular traveling wave solutions behave as attractors.

We impose a symmetric upstream–downstream profile with $u_{\mathrm{Left}}=-u_{\mathrm{Right}}=u_1>0$. One integration of (3.2) results with

$$\frac{u^2}{2}-\frac{u_1^2}{2}=-\delta u_{xx}^2,$$

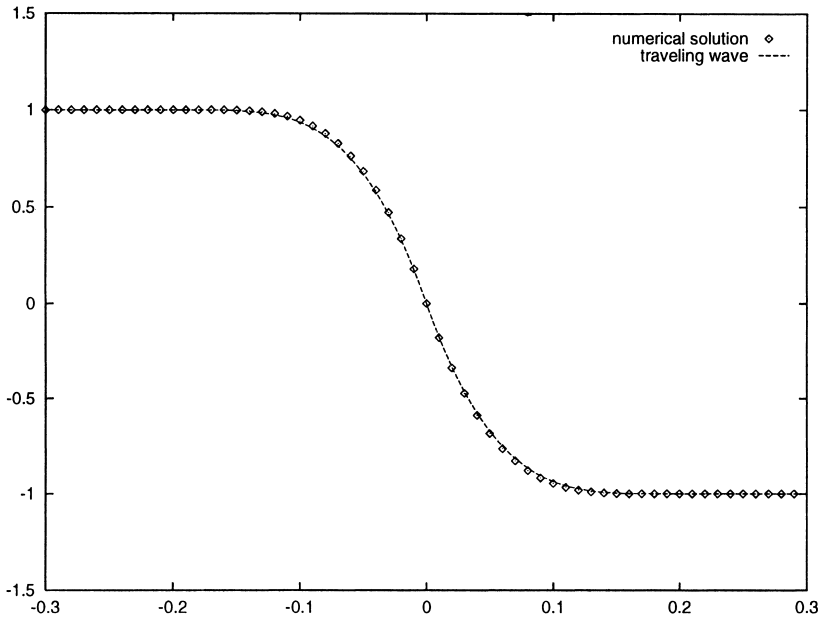

Fig. 1. Convergence of the numerical solution to the traveling wave solution, $\delta = 10^{-5}$, $T = 0.5$.

which can be integrated twice to yield

$$x = -(2\delta)^{1/4} \int_0^u \left(\pm \left(s\sqrt{u_1^2 - s^2} + u_1^2 \arcsin\left(\frac{s}{u_1}\right) - \frac{\pi}{2} u_1^2 \right) \right)^{-1/2} \mathrm{d}s. \tag{3.3}$$

The sign in the integrand is set according to the sign of u. In particular, for $u_1 = 1$, (3.3) becomes

$$x = -(2\delta)^{1/4} \int_0^u \left(\pm \left(s\sqrt{1 - s^2} + \arcsin s - \frac{\pi}{2} \right) \right)^{-1/2} \mathrm{d}s. \tag{3.4}$$

We demonstrate this profile in the following example in which we approximate solutions of (3.2) using the numerical scheme presented in Section 2.2. Here, we used Riemann initial data as

$$u_0(x) = \begin{cases} 1, & x < 0, \\ -1, & x > 0. \end{cases} \tag{3.5}$$

The results are plotted in Figs. 1 and 2 for different values of δ, after the steady-state was reached. These numerical results hint that the traveling wave solutions behave as attractors to the approximate solutions.

3.2. The one-sided Lipschitz condition

It is surprisingly easy to derive a formal one-sided bound on the derivative u_x in (2.3). Here, we have to augment (2.3) with additional assumptions on $g(s)$ given in the following elementary lemma:

Lemma 3.1 (OSLC). *Consider* (2.3). *Assume that* $\forall s,\ f''(s) > 0, g''(s) < 0$ *and that* $g'(0) = 0$. *Then the derivative,* u_x, *satisfies the formal one-sided estimate*

$$\max_x u_x(t) \leq \max_x u_x(0), \quad \forall t > 0. \tag{3.6}$$

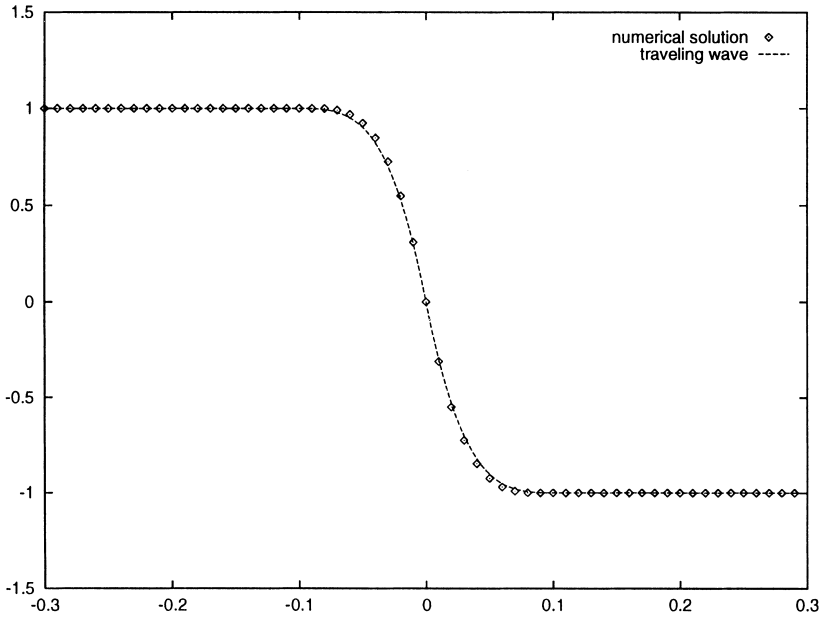

Fig. 2. Convergence of the numerical solution to the traveling wave solution, $\delta = 10^{-6}$, $T = 0.5$.

Proof. Differentiating (2.3) once yields

$$u_{tx} + (f'(u)u_x)_x - \delta(g'(u_{xx})u_{xxx})_x = 0. \tag{3.7}$$

Denoting $w = u_x$, (3.7) can be rewritten as

$$w_t + f''(u)w^2 + f'(u)w_x - \delta g''(w_x)w_{xx}^2 - \delta g'(w_x)w_{xxx} = 0.$$

If we now take $v(t) = \max_x w(x, t)$, then due to the assumptions of the lemma, $\dot{v} < 0$ and (3.6) follows. □

The appearance of a fourth-order derivative in (2.7), (2.8) and (2.9) prevents us from writing an analog of Lemma 3.1 in this case. The fact that the fourth-order derivative appears with the "correct" negative sign in the RHS of the equations is associated with a dissipative process, but to quantify this in terms of the desired bound on the derivative seems to be a highly non-trivial task.

4. Strong convergence?

In this section we numerically study the limit of solutions of (2.2) and (2.3) as the parameter δ tends to zero. Our starting point is the results obtained by approximating solutions of (3.1) subject to the exponentially decaying initial conditions $u(x, 0) = \mathrm{e}^{-100x^2}$. Similar phenomena to those we describe below, appear with other choices of initial data.

Fig. 3 presents our most interesting discovery. One can observe the creation of a *single* dispersive "ripple" which *disappears* as $\delta \to 0$. This phenomenon is totally different from what we know about solutions of dispersive equations (KdV-type). There, an infinite dispersive wave-train develops in time (compare, e.g., with [2], p. 64). This wave-train increases at the same limit $\delta \to 0$. In that limit, the solution appears to strongly converge to the entropy solution of the Burgers equation subject to the same initial data.

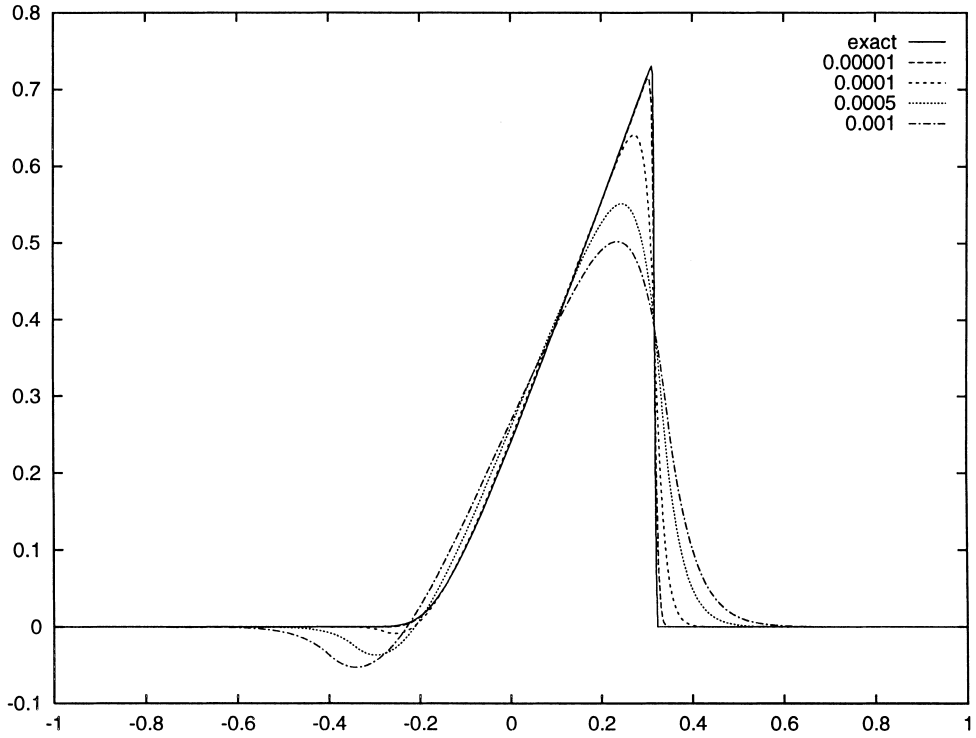

Fig. 3. Absolute-value dispersion with exponential initial data. $N = 400$, $T = 0.5$, $\Delta t \cdot \delta = 10^{-8}$. The different plots refer to different values of δ. The "exact" curve is the entropy solution of the Burgers equation subject to the same initial data.

We confirm that the results shown in Fig. 3 are independent of the spatial spacing Δx, by demonstrating in Fig. 4 a case in which δ is being held fixed while approaching the limit $\Delta x \to 0$.

The evolution in time of the solution is shown in Fig. 5. We note that the dispersive ripple does not increase in magnitude above a certain size (which by Fig. 3 is determined by the value of δ). No other ripples are being developed.

In Fig. 6 we present a fully numerical phenomenon in which spurious oscillations propagate from the shock. This happens when the equation is numerically solved for a relatively small value of δ and a relatively large Δx. We observe that these oscillations disappear as $\Delta x \to 0$. A further study of similar numerical phenomena is presented in Section 5.

A single ripple which disappears as δ tends to zero is observed when Eq. (3.1) is replaced by the smoother variant (3.2) subject to the same exponential initial data. An example of the approximated solutions of (3.2) is presented in Fig. 7. Once again we observe the appearance of a single dispersive ripple which vanishes in the limit $\delta \to 0$. As before, in that limit, the solution appears to strongly converge to the unique entropy solution of the Burgers equation subject to the same initial data.

Our numerical results in this section lead us to the following

Conjecture 4.1. *The solution of*

$$u_t + f(u)_x - \delta g(u_{xx})_x = -\epsilon u_{xxxx}, \qquad \delta, \epsilon > 0,$$

with a strictly convex f and a concave g, with $g(0) = 0$, *strongly converges to the unique entropy solution of* (1.1) *as* δ *and* $\epsilon\delta^{-1}$ *tend to* 0.

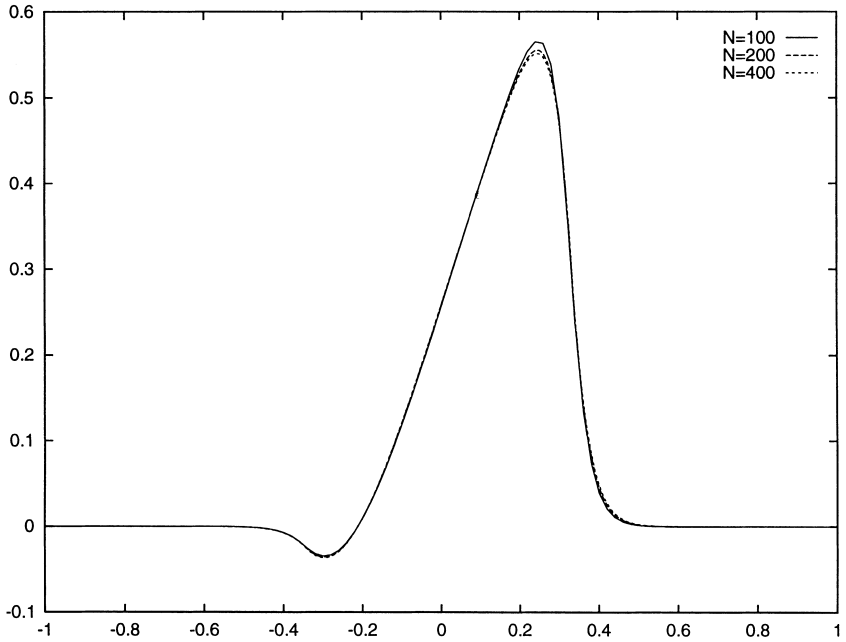

Fig. 4. Absolute-value dispersion with exponential initial data. $\delta = 5 \times 10^{-4}, T = 0.5$. For $N = 400, \Delta t = 2 \times 10^{-5}$. For $N = 200, \Delta t = 2 \times 10^{-4}$. For $N = 100, \Delta t = 2 \times 10^{-3}$.

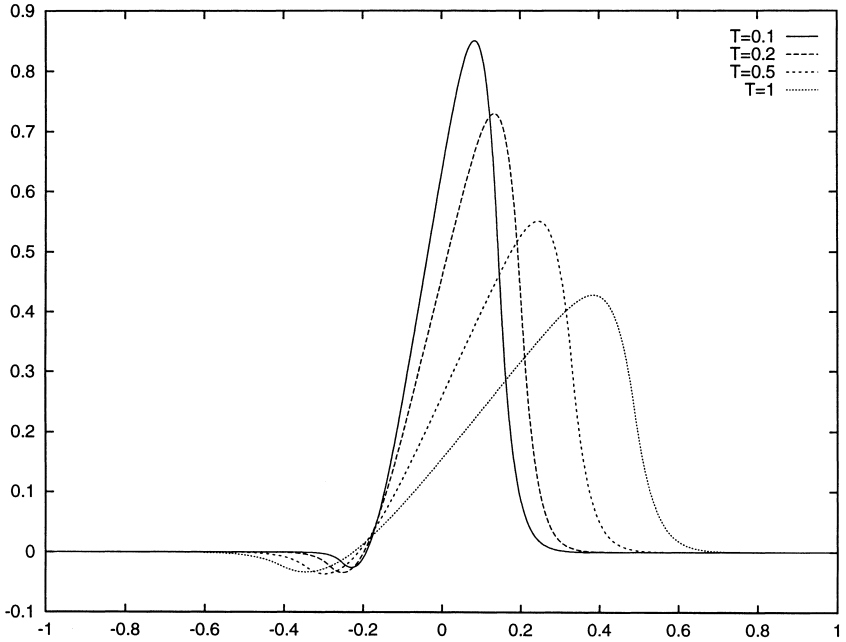

Fig. 5. Absolute-value dispersion with exponential initial data. Time evolution of the solution. $N = 400, \delta = 5 \times 10^{-4}, \Delta t = 2 \times 10^{-5}$.

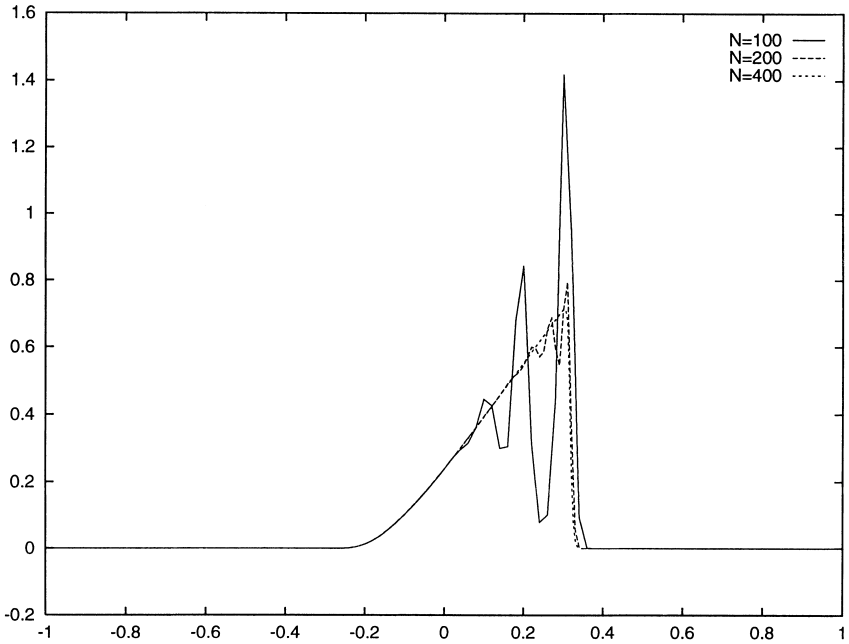

Fig. 6. Absolute-value dispersion with exponential initial data. The appearance of numerical oscillations for small $\delta = 10^{-5}$, $T = 0.5$. For $N = 200$, $\Delta t = 10^{-4}$. For $N = 100$, $\Delta t = 10^{-3}$.

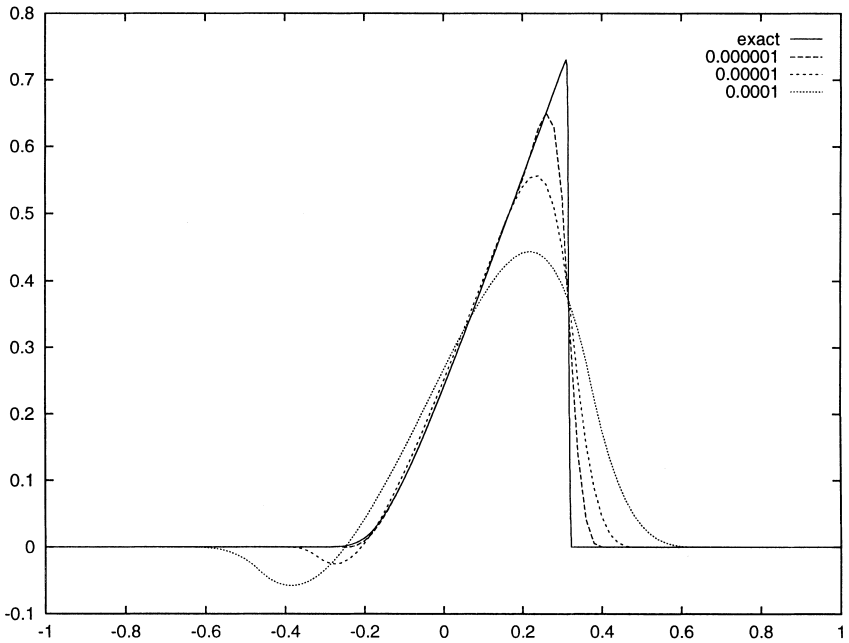

Fig. 7. Smooth dispersion with exponential initial data. $N = 400$, $T = 0.5$, $\Delta t \cdot \delta = 10^{-8}$. The different plots refer to different values of δ The "exact" curve is the entropy solution of the Burgers equation subject to the same initial data.

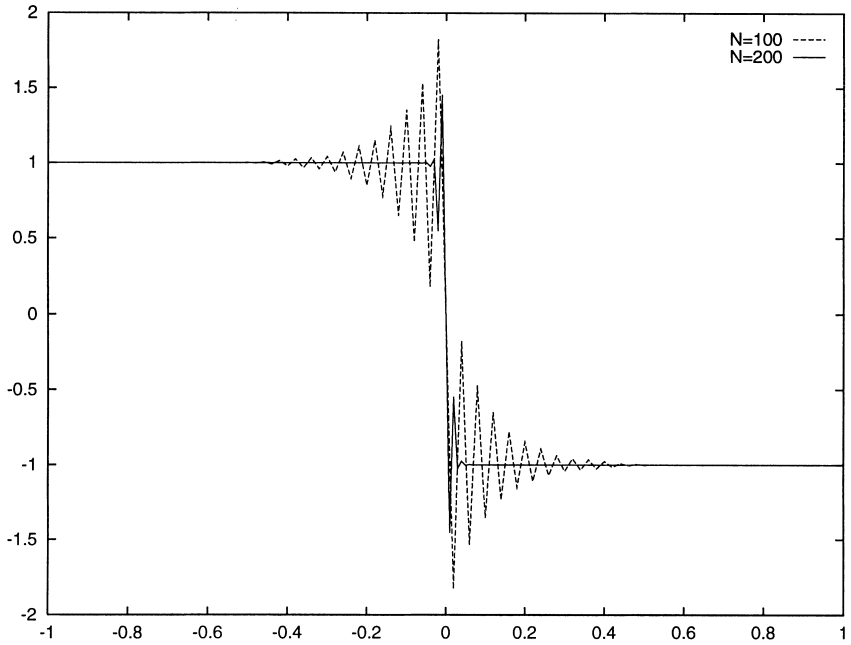

Fig. 8. Absolute-value dispersion with Riemann initial data. $\delta = 10^{-5}$, $T = 0.5$.

5. Study of the spurious numerical oscillations

In this section we demonstrate and analyze several cases in which numerical oscillations appear. We emphasize that the goal of this study is to gain a better understanding in order to distinguish between the properties of the model equations and the phenomena which are strictly related to the numerics in hand.

In Figs. 8–10 we present results obtained by approximating solutions of (2.3) with $g(u_{xx}) = -|u_{xx}|$, subject to the Riemann initial data (3.5) for several different sets of parameters.

One can clearly observe the binary oscillations propagating from the discontinuity at the center of the domain. These oscillations are strictly associated with the numerical method.

Note, in particular, the difference between the two oscillatory solutions presented in Fig. 9. While the support of the oscillations of the solution for $N = 100$ expand in time, the solution for $N = 200$ is a steady-state. Even though we do not know what mechanism toggles between these two states, we are able in the steady-state case to compute the envelope of the decaying oscillations.

We would like to stress that these oscillations appear in the non-smooth $g(s) = -|s|$, but do not appear with the smoother $g(s) = -s^2$. Such oscillations-free results were already presented in the study of traveling waves with the smooth $g(s) = -s^2$ (Figs. 1 and 2).

The numerical initial data which were used in Figs. 8–10 includes the origin $(0, 0)$. The existence of this point in the initial data has a strong stabilizing effect on the results. It seems to control the oscillations such that they do not change sign and they remain bounded in time. This is not the case when this extra point is not used. For comparison we bring in Figs. 11–13 equivalent results to Figs. 8–10 when no such extra point is used. Similar sensitivity of the oscillations with respect to the location of the grid points was previously observed in a different context by Hayes in [5].

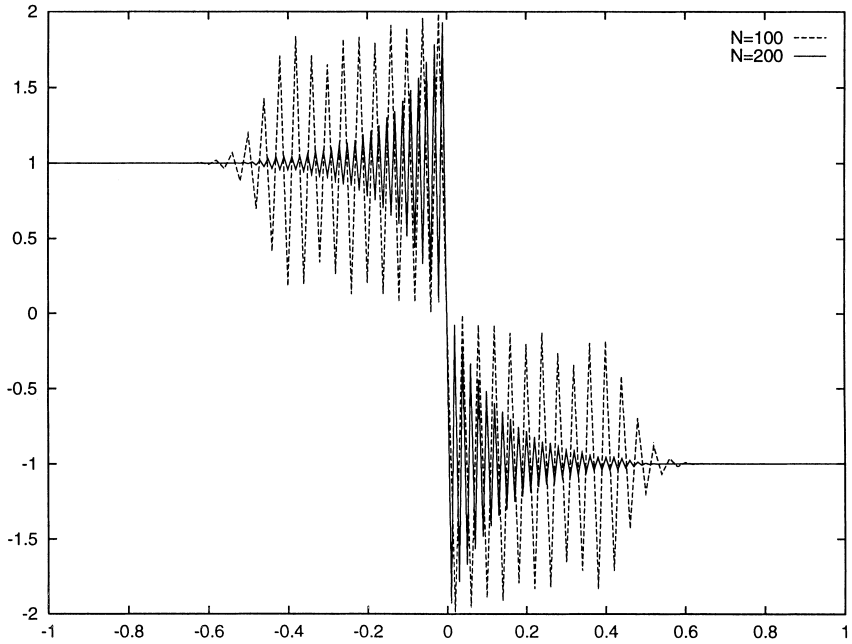

Fig. 9. Absolute-value dispersion with Riemann initial data. $\delta = 10^{-6}$, $T = 0.5$.

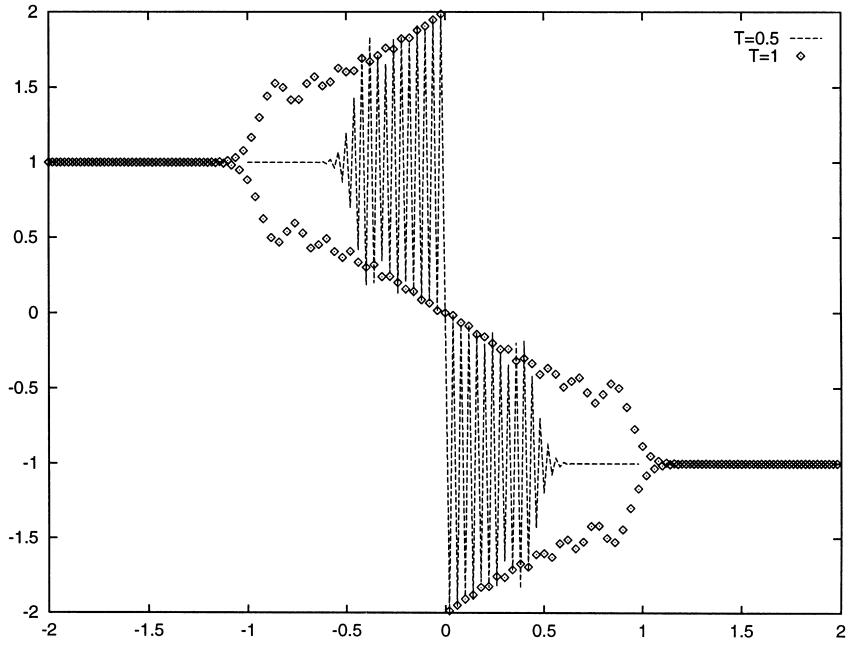

Fig. 10. Absolute-value dispersion with Riemann initial data. $\delta = 10^{-6}$, $N = 100$.

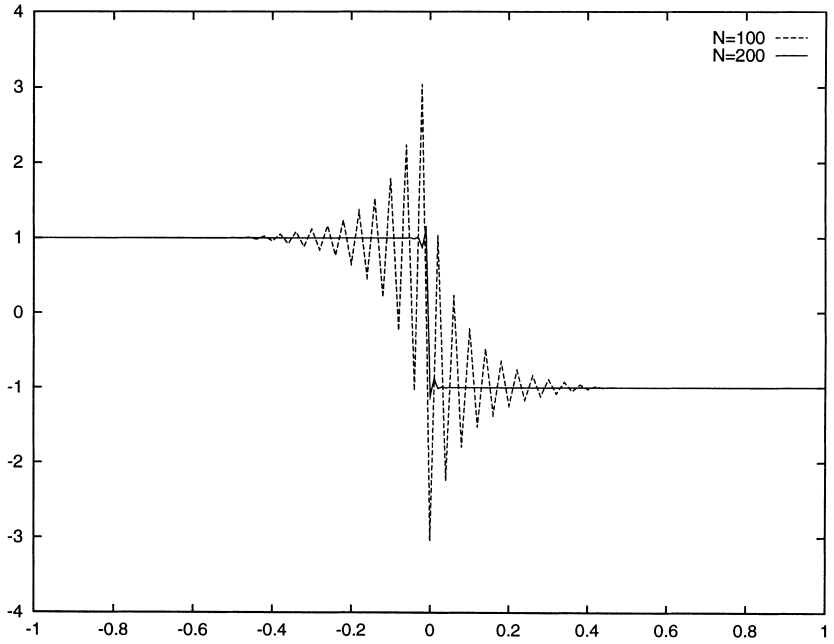

Fig. 11. Absolute-value dispersion with Riemann initial data which does not include the origin. $\delta = 10^{-5}$, $T = 0.5$.

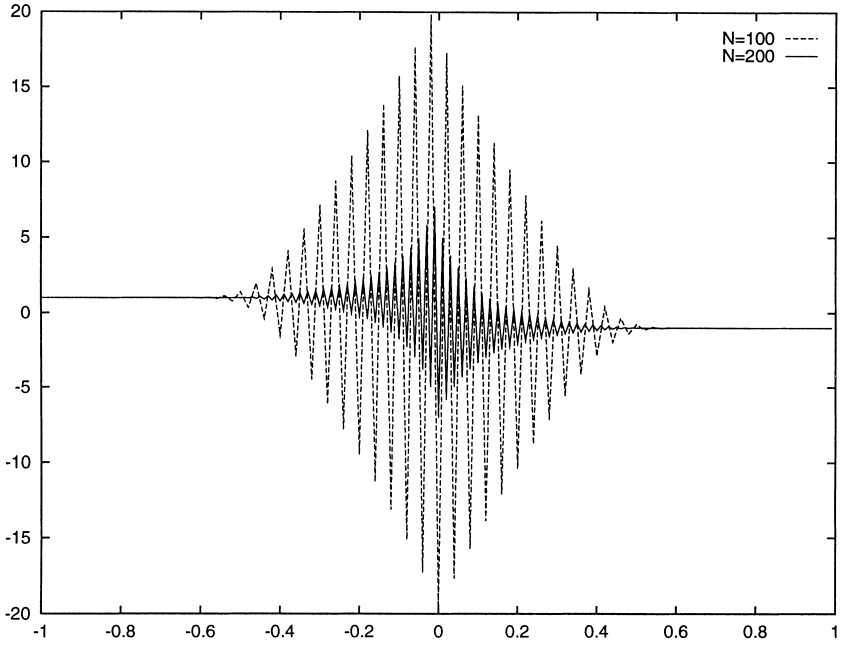

Fig. 12. Absolute-value dispersion with Riemann initial data which does not include the origin. $\delta = 10^{-6}$, $T = 0.5$.

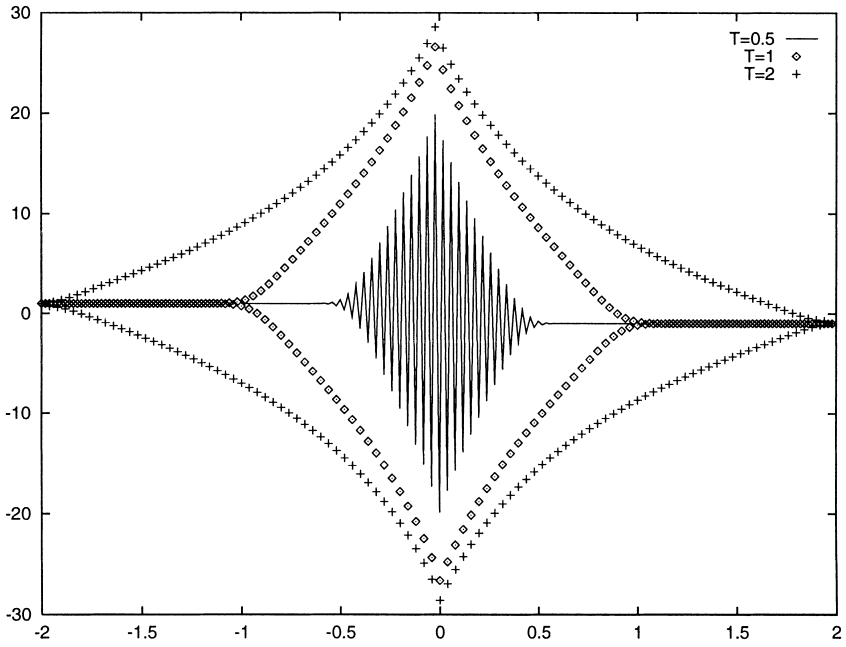

Fig. 13. Absolute-value dispersion with Riemann initial data which does not include the origin. $\delta = 10^{-6}$, $N = 100$.

We turn to a study of the binary oscillations presented in the above examples. The method we use follows the lines of Goodman and Lax in [3]. Similar techniques were used, e.g., in [4,5,7].

Our starting point is the method of lines (2.5) with the specific choice of $f(u) = u^2/2$. We assume that the numerical solution introduces binary oscillations of the form

$$u_i = v_i + (-1)^i w_i. \tag{5.1}$$

We plug (5.1) into (2.5). For the first term, we have

$$\begin{aligned}\frac{1}{\Delta x}\,\Delta_-\left[f\left(\frac{u_i+u_{i+1}}{2}\right)\right] &= \frac{1}{8\Delta x}[(u_{i+1}+u_{i-1}+2u_i)(u_{i+1}-u_{i-1})]\\ &= \begin{cases}\dfrac{v_{i+1}-w_{i+1}+v_{i-1}-w_{i-1}+2v_i+2w_i}{4}\,\dfrac{v_{i+1}-v_{i-1}-w_{i+1}+w_{i-1}}{2\Delta x}, & i \text{ even},\\ \dfrac{v_{i+1}+w_{i+1}+v_{i-1}+w_{i-1}+2v_i-2w_i}{4}\,\dfrac{v_{i+1}-v_{i-1}+w_{i+1}-w_{i-1}}{2\Delta x}, & i \text{ odd},\end{cases}\end{aligned} \tag{5.2}$$

If we consider Eq. (5.2) as a discrete approximation of continuous equation, it can be rewritten as

$$\frac{1}{\Delta x}\Delta_-\left[f\left(\frac{u_i+u_{i+1}}{2}\right)\right] \to \begin{cases} v(v_x-w_x), & i \text{ even},\\ v(v_x+w_x), & i \text{ odd}.\end{cases} \tag{5.3}$$

For the second term in (2.5) we repeat the same analysis and end with

$$\Delta_- g(w_i, w_{i+1}) \to \begin{cases} g\left(v_{xx}-\dfrac{4w}{(\Delta x)^2}, v_{xx}+\dfrac{4w}{(\Delta x)^2}\right) - g\left(v_{xx}+\dfrac{4w}{(\Delta x)^2}, v_{xx}-\dfrac{4w}{(\Delta x)^2}\right), & i \text{ even},\\ g\left(v_{xx}+\dfrac{4w}{(\Delta x)^2}, v_{xx}-\dfrac{4w}{(\Delta x)^2}\right) - g\left(v_{xx}-\dfrac{4w}{(\Delta x)^2}, v_{xx}+\dfrac{4w}{(\Delta x)^2}\right), & i \text{ odd}.\end{cases} \tag{5.4}$$

When we specifically choose the flux-limiter as the Engquist–Osher (EO) limiter, (5.4) becomes

$$\Delta_- g(w_i, w_{i+1}) \to \begin{cases} \operatorname{sgn}(\alpha)g(\alpha) - \operatorname{sgn}(\beta)g(\beta), & i \text{ even}, \\ -\operatorname{sgn}(\alpha)g(\alpha) + \operatorname{sgn}(\beta)g(\beta), & i \text{ odd}. \end{cases} \tag{5.5}$$

where

$$\alpha = v_{xx} + \frac{4w}{(\Delta x)^2}, \qquad \beta = v_{xx} - \frac{4w}{(\Delta x)^2}. \tag{5.6}$$

We require that the continuous solution will satisfy both equation for the even and odd indices. Combining the results of (5.3) and (5.5), the continuous equations that correspond to the discretization of the method of lines (2.5) given by the binary oscillations solution (5.1) are

$$\begin{aligned} &(v+w)_t + v(v_x - w_x) - \frac{\delta}{\Delta x}(\operatorname{sgn}(\alpha)g(\alpha) - \operatorname{sgn}(\beta)g(\beta)) = 0, \\ &(v-w)_t + v(v_x + w_x) - \frac{\delta}{\Delta x}(-\operatorname{sgn}(\alpha)g(\alpha) + \operatorname{sgn}(\beta)g(\beta)) = 0, \end{aligned} \tag{5.7}$$

where α and β are given in (5.6). If we specifically chose $g(s) = -|s|$ then for $v_{xx} \ll 4w/(\Delta x)^2$, (5.7) becomes

$$(v+w)_t + v(v_x - w_x) + \frac{8\delta}{(\Delta x)^3}w = 0, \quad (v-w)_t + v(v_x + w_x) - \frac{8\delta}{(\Delta x)^3}w = 0. \tag{5.8}$$

Here, it is clear that by taking the limit $\delta \to 0$, in order not to affect the oscillations that might develop, the ratio $\delta/(\Delta x)^3$ has to be held fixed. Of course, numerically in this case, the RHS has a term $-\epsilon u_{xxxx}$, with $\epsilon = \Delta x\delta$ which is of order $\delta/(\Delta x)^3$. Taking δ large enough for a fixed Δx means that there is more dissipation and in such a way oscillations can be controlled.

An example of such sort of control of the oscillations is shown in Fig. 14. Here, we approximated the solution of (3.1), subject to the Riemann initial data (3.5). The ratio $\delta/(\Delta x)^3$ was held fixed.

As previously noted, in several cases when binary oscillations appear, it seems as if there is convergence to steady-state solutions. The envelope of this steady-state solutions can be computed from the above analysis, since what we are left with in this case amounts to (assuming positive $w > 0$)

$$v_t + vv_x = 0, \quad w_t - vw_x + cw = 0, \tag{5.9}$$

where $c = 8\delta/(\Delta x)^3$. Then, for $\partial_t = 0$, we have

$$v^s v_x^s = 0, \quad -v^s w_x^s + cw^s = 0. \tag{5.10}$$

Hence, $v^s = \pm\tilde{c}$ which can be determined by taking the limit $x \to \pm\infty$. For the particular choice of $v^s = \pm 1$ one has

$$w^s = \pm\hat{c}\mathrm{e}^{\pm cx} = \pm\hat{c}\mathrm{e}^{\pm(8\delta/(\Delta x)^3)x}.$$

We experimentally observed that when the initial data includes the origin, the oscillations do not change sign and hence $\hat{c}$ is limited by the size of the discontinuity. The envelope of the oscillations is therefore given by

$$v \pm w = \pm 1 \pm \mathrm{e}^{\pm(8\delta/(\Delta x)^3)x},$$

where the different variations of the sign correspond to the upper/lower envelope at each part of the solution.

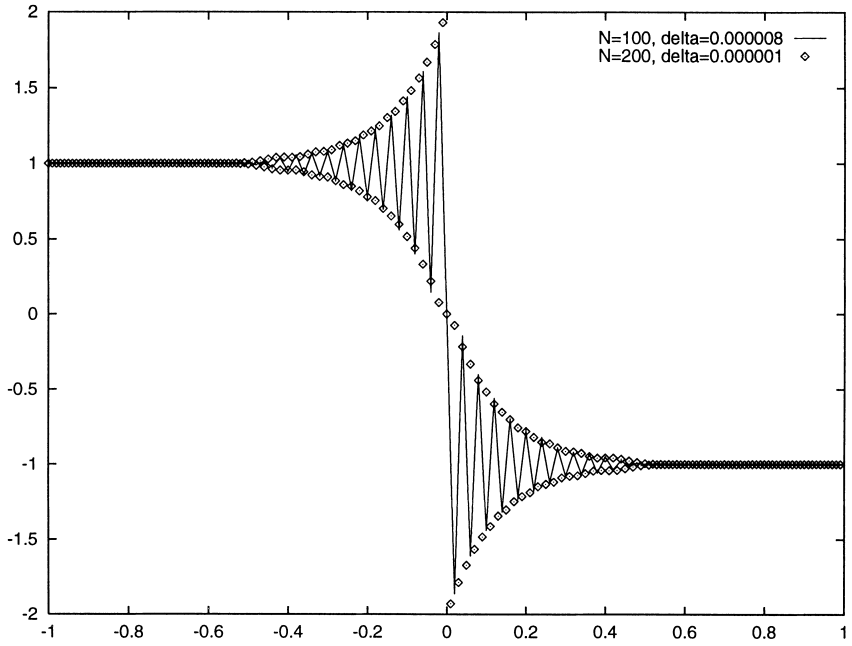

Fig. 14. Steady-state solution, $T = 0.5$. Fixed $\delta/(\Delta x)^3$ controls the oscillations.

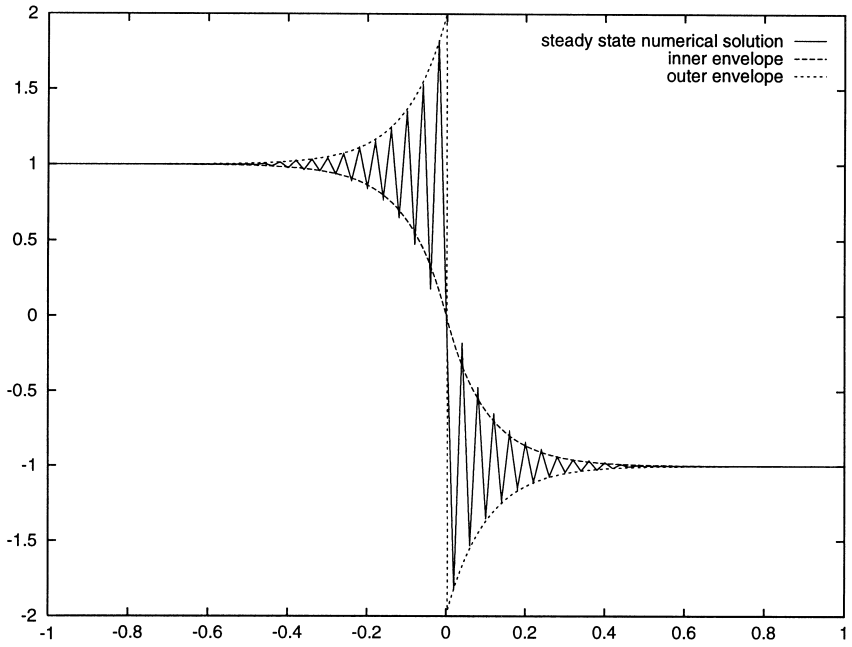

Fig. 15. The envelope of the steady-state oscillatory solution, $N = 100$, $\delta = 10^{-5}$, $T = 0.5$.

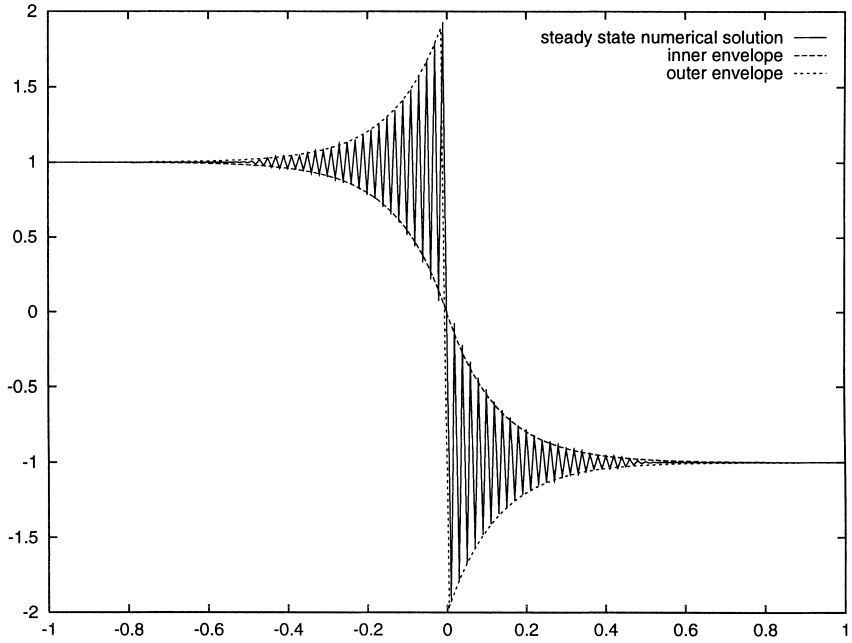

Fig. 16. The envelope of the steady-state oscillatory solution, $N = 200$, $\delta = 10^{-6}$, $T = 0.5$.

In Figs. 15 and 16 we plot the results obtained by solving (3.1) subject to the Riemann initial data (3.5). The numerical solution convergence to an oscillatory steady-state solution in which the oscillation are binary.

In Fig. 15, the parameters used were $\delta = 10^{-5}$, $N = 100$. The corresponding outer envelope takes the form

$$\begin{cases} -1 + \mathrm{e}^{-cx}, & x > 0, \\ 1 - \mathrm{e}^{-cx}, & x < 0, \end{cases} \qquad c = 10,$$

while the inner envelope is

$$\begin{cases} -1 - \mathrm{e}^{-cx}, & x > 0, \\ 1 + \mathrm{e}^{-cx}, & x < 0. \end{cases} \qquad c = 10,$$

In Fig. 16, the parameters were changed to $\delta = 10^{-6}$, $N = 200$. The corresponding outer envelope takes the same form, with a different constant $c = 8$.

Acknowledgements

The research was supported in part by TMR grant #ERBFMRXCT960033. The work of D.L. was supported in part by the Applied Mathematical Sciences subprogram of the Office of Science, U.S. Department of Energy, under contract DE-AC03-76-SF00098. Part of the research was done while D.L. was affiliated with ENS Paris. D.L. would like to thank E. Tadmor and A. Kurganov for stimulating discussions.

References

[1] Y. Brenier, S. Osher, The discrete one-sided Lipschitz condition for convex scalar conservation laws, SINUM 25 (1) (1988) 8–23.
[2] P.G. Drazin, Solitons, London Math. Soc. Lect. Note Ser. 85, Cambridge University Press, Cambridge, 1983.
[3] J. Goodman, P.D. Lax, On dispersive difference schemes, I, Commun. Pure Appl. Math. 41 (1988) 591–613.
[4] B.T. Hayes, Binary and ternary oscillations in a cubic numerical scheme, Physica D 120 (1998) 287–314.
[5] B.T. Hayes, Binary modulated oscillations in a semi-discrete version of Burgers equation, Physica D 106 (1997) 287–313.
[6] P.D. Lax, C.D. Levermore, The small dispersion limit of the Korteweg–de Vries equation, III, Commun. Pure Appl. Math. 36 (1983) 809–829.
[7] C.D. Levermore, J.-G. Liu, Large oscillations arising in a dispersive numerical scheme, Physica D 99 (1996) 191–216.
[8] R.J. LeVeque, Numerical Methods for Conservation Laws, Lectures in Mathematics, ETH Zürich, Birkhäuser, Basel, 1992.
[9] D. Serre, Systèmes de Lois de Conservation, I, Diderot Editeur, Paris, 1996.
[10] J. Smoller, Shock Waves and Reaction–Diffusion Equations, Springer, Berlin, 1983.
[11] G.B. Whitham, Linear and Nonlinear Waves, Wiley/Interscience, New York, 1974.